



# ***GW* study of topological insulators $\text{Bi}_2\text{Se}_3$ , $\text{Bi}_2\text{Te}_3$ , and $\text{Sb}_2\text{Te}_3$ : Beyond the perturbative one-shot approach**

Irene Aguilera, Christoph Friedrich, Gustav Bihlmayer, and Stefan Blügel

*Peter Grünberg Institute and Institute for Advanced Simulation, Forschungszentrum Jülich and JARA, D-52425 Jülich, Germany*

(Received 25 June 2013; published 29 July 2013)

We present *GW* calculations of the topological insulators  $\text{Bi}_2\text{Se}_3$ ,  $\text{Bi}_2\text{Te}_3$ , and  $\text{Sb}_2\text{Te}_3$  within the all-electron full-potential linearized augmented-plane-wave formalism. Quasiparticle effects produce significant qualitative changes in the band structures of these materials when compared to density functional theory (DFT), especially at the  $\Gamma$  point, where band inversion takes place. There, the widely used perturbative one-shot *GW* approach can produce unphysical band dispersions, as the quasiparticle wave functions are forced to be identical to the noninteracting single-particle states. We show that a treatment beyond the perturbative approach, which incorporates the off-diagonal *GW* matrix elements and thus enables many-body hybridization to be effective in the quasiparticle wave functions, is crucial in these cases to describe the characteristics of the band inversion around the  $\Gamma$  point in an appropriate way. In addition, this beyond one-shot *GW* approach allows us to calculate the values of the  $Z_2$  topological invariants and compare them with those previously obtained within DFT.

DOI: [10.1103/PhysRevB.88.045206](https://doi.org/10.1103/PhysRevB.88.045206)

PACS number(s): 71.10.-w, 71.15.Mb, 71.20.-b, 71.70.Ej

## I. INTRODUCTION

Recently, the concept of a new kind of insulator, the topological insulator, was developed.<sup>1-5</sup> This paved the way for new physics with new electronic phenomena and a great potential for applications in spintronics, quantum computing, thermoelectrics, or Green IT, due to the possibility of generation and control of dissipationless spin currents.<sup>6-8</sup> In topological insulators, a strong spin-orbit interaction causes an inversion of electronic bands and gives rise to nontrivial edge or surface states that, by symmetry considerations, are required to be metallic. Moreover, the conducting edges and surfaces have several special features with respect to their transport properties. These conducting states realizing the metallic surfaces or edges are protected by time-reversal symmetry in the sense that electron propagation is dissipationless because the backscattering of charge carriers is forbidden as long as the topological properties are intact.<sup>9</sup>

Among topological insulators, the family formed by  $\text{Bi}_2\text{Se}_3$ ,  $\text{Bi}_2\text{Te}_3$ , and  $\text{Sb}_2\text{Te}_3$  is one of the most widely studied due to the simplicity of their surface states consisting of a single Dirac cone at the  $\Gamma$  point.<sup>10</sup> Their experimental band gaps between 0.15 and 0.30 eV make them good candidates for experimental studies of topological effects and for room-temperature applications. In addition, these materials and some of their alloys are nowadays commonly used in thermoelectric refrigeration and power generation.<sup>11,12</sup>

Most of the calculations present in the literature for this family of materials have been based on model Hamiltonians or parameter-dependent tight-binding descriptions,<sup>1,13-15</sup> and density functional theory (DFT) employing the local-density (LDA) or generalized gradient (GGA) approximations.<sup>11,16-23</sup> The LDA and GGA functionals, due to their efficiency, have allowed for the study of surface states of these materials.<sup>10,24-27</sup> However, these functionals are made for the electronic ground state, and it is known that they are not appropriate for band gaps and excited-state properties, such as the quasiparticle (QP) band structure.

To overcome this problem, we employ many-body perturbation theory in the *GW* approximation<sup>28</sup> to calculate

quasiparticle self-energy corrections for the electronic states, which yields results that are directly comparable to photoemission spectroscopy measurements. Recently, *GW* calculations on  $\text{Bi}_2\text{Se}_3$  and  $\text{Bi}_2\text{Te}_3$  have shown<sup>29-31</sup> that not only a much better agreement of the band gap but also an improvement in the effective masses is found when comparing to experimental results. We have performed one-shot *GW* calculations for  $\text{Bi}_2\text{Se}_3$ ,  $\text{Bi}_2\text{Te}_3$ , and  $\text{Sb}_2\text{Te}_3$  within the all-electron full-potential linearized augmented-plane-wave (FLAPW) method.

The one-shot *GW* quasiparticle correction is usually applied in a perturbative approach, where the QP wave functions are approximated by the corresponding Kohn-Sham (KS) single-particle states, as this requires only the diagonal elements of the *GW* self-energy to be calculated. However, we demonstrate in this work that this leads to unphysical QP band dispersions, especially in regions of the Brillouin zone where hybridization is strongly affected by *GW* corrections as, for example, in the band-inverted region close to the  $\Gamma$  point. These unphysical dispersions are caused by the neglect of hybridization effects that arise from the off-diagonal part of the self-energy. In fact, going beyond the perturbative approach and thus allowing for changes in the QP wave functions immediately rectifies the band dispersions, which become smooth and physical.

In addition, the inclusion of the off-diagonal elements of the self-energy allows us to obtain the *GW* quasiparticle wave functions and discuss properties derived from them, like the band inversion and the  $Z_2$  topological invariants.<sup>1,4</sup>

## II. METHODS AND COMPUTATIONAL DETAILS

All calculations were carried out within the all-electron FLAPW formalism as implemented in the DFT code FLEUR<sup>32</sup> and the *GW* code SPEX.<sup>33</sup> The FLAPW method treats core, valence, and conduction electrons on an equal footing.

The electron density is determined self-consistently employing the Perdew-Zunger parametrization of the LDA exchange-correlation functional.<sup>34</sup> The core electrons are

treated fully relativistically by solving the Dirac equation with the spherically averaged effective potential around each nucleus. For the valence electrons, space is partitioned into muffin-tin (MT) spheres and an interstitial region; in the former we use an angular momentum cutoff  $l_{\max} = 10$  and in the latter a plane-wave cutoff of  $4.5 \text{ bohrs}^{-1}$ . In the MT spheres, relativistic effects are included in the scalar-relativistic approximation,<sup>35</sup> while the spin-orbit coupling (SOC) is incorporated self-consistently employing the “second variation” technique.<sup>36</sup> An  $8 \times 8 \times 8$   $\mathbf{k}$ -point grid was used to sample the Brillouin zone.

For the  $GW$  calculations, a mixed product basis<sup>33,37</sup> is used to represent the two-particle quantities, such as the dielectric matrix and the screened interaction. It is constructed with an angular momentum cutoff of  $l = 5$  and a linear momentum cutoff of  $2.9 \text{ bohrs}^{-1}$ . We have carried out a thorough study of the convergence with the number of unoccupied bands and  $\mathbf{k}$ -point samplings. All  $GW$  results are obtained with a  $4 \times 4 \times 4$   $\mathbf{k}$ -point sampling. To compute the Green function and the polarization function, we use 500 bands for  $\text{Bi}_2\text{Se}_3$  and  $\text{Bi}_2\text{Te}_3$  and 800 bands for  $\text{Sb}_2\text{Te}_3$ . This corresponds to approximately 80 eV above the Fermi energy for  $\text{Bi}_2\text{Se}_3$  and  $\text{Bi}_2\text{Te}_3$  and 140 eV for  $\text{Sb}_2\text{Te}_3$ . With these parameters, the band gaps are converged to within 10 meV.

In all cases, semicore  $d$  states of Se, Te, Bi, and Sb are treated as valence orbitals by the use of local orbitals. To describe high-lying states accurately and avoid linearization errors,<sup>38,39</sup> we include for each atom two local orbitals (three in the case of  $\text{Sb}_2\text{Te}_3$ ) per angular momentum up to  $l = 3$ . For all the band diagrams shown in this work, self-energy corrections have been calculated on a dense linear  $\mathbf{k}$ -point grid; no interpolation technique has been used. In each case, the Fermi level is placed in the middle of the band gap. We use the experimental lattice structures of Refs. 40 ( $\text{Bi}_2\text{Se}_3$ ), 41 ( $\text{Bi}_2\text{Te}_3$ ), and 42 ( $\text{Sb}_2\text{Te}_3$ ).

In contrast to previous calculations,<sup>29,30</sup> we take account of the SOC already in the reference system so that the single-particle states entering the Green function and the screened interaction are given by four-component spinor wave functions, as obtained from a DFT calculation including spin-orbit coupling. The spinor wave functions give rise to spin-off-diagonal blocks in the Green function and the self-energy,<sup>43</sup> the coupling of the spin channels being mediated by the spin-orbit interaction. This allows for spin-flip processes and many-body renormalization of the spin-orbit coupling itself.<sup>44</sup> The screened interaction is calculated within the random-phase approximation without resorting to a plasmon-pole model for the frequency dependence. The frequency convolution of the self-energy is evaluated with the use of a contour integration technique on the complex frequency plane.<sup>45,46</sup>

In many-body perturbation theory, the quasiparticle wave functions  $\psi_{\mathbf{k}\nu}(x)$  and energies  $\varepsilon_{\mathbf{k}\nu}^{\text{QP}}$  satisfy the Schrödinger-like equation

$$[\hat{T} + v_{\text{ext}}(\mathbf{r}) + v_{\text{H}}(\mathbf{r})]\psi_{\mathbf{k}\nu}(x) + \int \Sigma(x, x'; \varepsilon_{\mathbf{k}\nu}^{\text{QP}})\psi_{\mathbf{k}\nu}(x')dx' = \varepsilon_{\mathbf{k}\nu}^{\text{QP}}\psi_{\mathbf{k}\nu}(x), \quad (1)$$

where  $\hat{T}$  is the relativistic kinetic energy operator including the SOC term,  $x = \{\mathbf{r}, \sigma\}$  is a composite variable comprising

space and spin variables,  $v_{\text{ext}}$  is the external potential,  $v_{\text{H}}$  the Hartree potential, and

$$\Sigma(x, x'; \omega) = \frac{i}{2\pi} \lim_{\eta \rightarrow 0^+} \int G(x, x'; \omega + \omega')W(\mathbf{r}, \mathbf{r}'; \omega')e^{i\eta\omega'}d\omega' \quad (2)$$

is the  $GW$  self-energy.<sup>28</sup> The Green function  $G$  and the screened interaction  $W$ , in formal notation  $W = (1 - vP)^{-1}v$  with  $P = -iGG$ , are defined with the help of a noninteracting reference system. We employ the Kohn-Sham system, in which the noninteracting electrons obey the equation of motion

$$[\hat{T} + v_{\text{ext}}(\mathbf{r}) + v_{\text{H}}(\mathbf{r}) + v_{\text{xc}}(\mathbf{r})]\phi_{\mathbf{k}\nu}(x) = \varepsilon_{\mathbf{k}\nu}^{\text{KS}}\phi_{\mathbf{k}\nu}(x) \quad (3)$$

with the exchange-correlation potential  $v_{\text{xc}}(\mathbf{r})$ , and the KS wave functions  $\phi_{\mathbf{k}\nu}(x)$  and energies  $\varepsilon_{\mathbf{k}\nu}^{\text{KS}}$ . The SOC term is treated within a second-variation technique where the KS Hamiltonian including SOC is diagonalized in the space of the KS states obtained without SOC.

In the perturbative one-shot  $GW$  approach, one utilizes the similarity of Eqs. (1) and (3) and assumes that  $\Sigma(\omega) - v_{\text{xc}}$  can be treated as a small perturbation. The quasiparticle energies are then given in first order by

$$\varepsilon_{\mathbf{k}\nu}^{\text{QP}} = \varepsilon_{\mathbf{k}\nu}^{\text{KS}} + \langle \phi_{\mathbf{k}\nu} | \Sigma(\varepsilon_{\mathbf{k}\nu}^{\text{QP}}) - v_{\text{xc}} | \phi_{\mathbf{k}\nu} \rangle, \quad (4)$$

where  $\langle \dots \rangle$  here denotes a double integration over space and a double spin summation, since the operator is nonlocal in  $x$ . This approximation is equivalent to assuming that  $\Sigma(\omega) - v_{\text{xc}}$  is band diagonal in the basis of the KS wave functions, or, synonymously, that the off-diagonal elements of  $\Sigma(\omega)$  are identical to those of  $v_{\text{xc}}$ . For most purposes it suffices to compute only the diagonal elements of the states of interest instead of the whole  $\Sigma$  matrix explicitly. However, we will show in this work that this simplification may lead to unphysical band dispersions in those parts of the Brillouin zone where the bands hybridize strongly. Examples include, but are not restricted to, states where the band inversion originates from strong SOC effects.

We go beyond the perturbative one-shot approach of Eq. (4) and solve Eq. (1) in the basis of KS states exactly, i.e., we calculate  $\Sigma(\omega)$  on a frequency mesh for  $\omega$  and as a full matrix  $\Sigma_{\nu\nu'}(\mathbf{k}, \omega) = \langle \phi_{\mathbf{k}\nu} | \Sigma(\omega) | \phi_{\mathbf{k}\nu'} \rangle$  with bands  $\nu$  and  $\nu'$  comprising the 18 highest occupied and 22 lowest unoccupied bands, which yields results converged to within 10 meV. A spline interpolation is employed for each matrix element of  $\Sigma(\omega)$  to interpolate between the frequency mesh points so that the nonlinear quasiparticle equation [Eq. (1)] can be solved for each quasiparticle state  $\nu$  by iteration, starting from the KS energy  $\omega = \varepsilon_{\mathbf{k}\nu}^{\text{KS}}$  in  $\Sigma(\omega)$  and reinserting the newly calculated eigenvalue in  $\Sigma(\omega)$  until self-consistency is achieved.<sup>47</sup> The self-consistent value  $\varepsilon_{\mathbf{k}\nu}^{\text{QP}}$  is then the quasiparticle energy. Since this procedure must be carried out for each state separately, the resulting quasiparticle wave functions are not eigenfunctions of the same operator. In particular, they are not orthogonal anymore, which is a characteristic of many-body quasiparticle amplitudes that cannot be interpreted as single-particle states.

### III. RESULTS

#### A. Calculations without SOC

The LDA and *GW* band structures of Bi<sub>2</sub>Se<sub>3</sub>, Bi<sub>2</sub>Te<sub>3</sub>, and Sb<sub>2</sub>Te<sub>3</sub> without SOC are compared in Figs. 1(a), 1(b), and 1(c), respectively. The panel (d) of the figure shows a magnification around the  $\Gamma$  point, where LDA predicts a “negative” band gap for Sb<sub>2</sub>Te<sub>3</sub>, resulting from an overlap of the valence band and conduction band. This can be seen from the size of the dark and light circles in the figure, which represents the orbital character of the two states. In the *GW* approximation, the bands separate and the band gap becomes positive. So, the strong LDA hybridizations that produce an avoided crossing of the bands in the vicinity of the  $\Gamma$  point should be removed in the *GW* result. However, due to the lack of off-diagonal elements in the perturbative one-shot *GW* approach [we label this approach “*GW* (diag)” in the following], a coupling that could *dehybridize* the bands is missing: an unphysical dispersion results where the avoided crossing occurs (black dashed lines). In fact, the inclusion

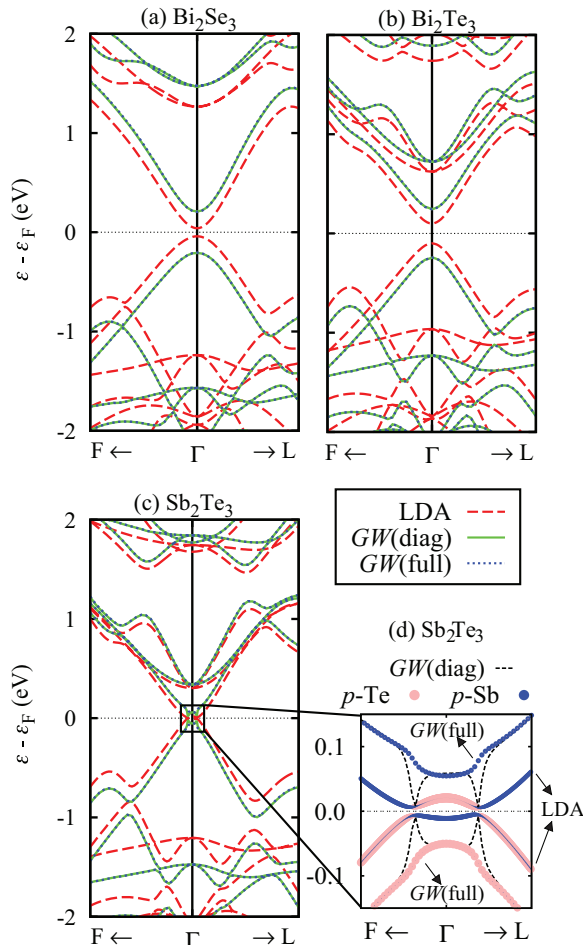


FIG. 1. (Color online) LDA, *GW* (diag), and *GW* (full) band structures of (a) Bi<sub>2</sub>Se<sub>3</sub>, (b) Bi<sub>2</sub>Te<sub>3</sub>, and (c) Sb<sub>2</sub>Te<sub>3</sub>, without SOC. The region around the  $\Gamma$  point in (c), where Eq. (4) [*GW* (diag)] yields unphysical results, is enlarged in (d). The size of the circles scales with the projections of the LDA and *GW* wave functions onto the *p* states of Sb (dark circles) and Te (light circles). The dashed-black lines in (d) show the *GW* (diag) eigenvalues for comparison.

of off-diagonal matrix elements in the self-energy operator [labeled “*GW* (full)”] correctly dehybridizes the bands. No avoided crossing occurs, and the wave functions acquire a pure orbital character, giving rise to a correct order of states. It should be noted that the orbital characters of the two states at the  $\Gamma$  point are (nearly) identical in LDA and *GW* (although in reversed order in energy), and as a result, the *GW* (diag) and *GW* (full) eigenvalues are (nearly) equal. The bands also coincide beyond the avoided-crossing region. The strong  $\mathbf{k}$  dependence of the screening induced by the avoided crossing of the LDA bands still gives rise to an unusually curved band dispersion in the *GW* (full) band structure. This is due to the self-interaction correction produced by the occupied *p*-Sb states in LDA that pulls the corresponding *GW* conduction band down, while, in the valence band, the *p*-Te states miss the self-interaction correction and are pushed up as a result. These unusual dispersions would probably disappear in a self-consistent *GW* calculation.

As can be seen from Figs. 1(a), 1(b), and 1(c), for Bi<sub>2</sub>Se<sub>3</sub> and Bi<sub>2</sub>Te<sub>3</sub>, and for states of Sb<sub>2</sub>Te<sub>3</sub> beyond the avoided crossing, the *GW* (diag) and *GW* (full) bands are indistinguishable on the scale of the figure.

For the three materials here studied, their topological properties are a result of the spin-orbit interactions and therefore it is crucial to include spin-orbit coupling in the calculation scheme. Most *GW* calculations with SOC in the literature have included the spin-orbit interactions *a posteriori* by adding them to a quasiparticle spectrum obtained in the absence of SOC. If such an approach is applied to Sb<sub>2</sub>Te<sub>3</sub>, it is clear from the above that the *GW* calculation has to be carried out taking into account the off-diagonal elements of  $\Sigma$  to avoid pathological band dispersions such as the ones shown as dashed lines in Fig. 1(d).

#### B. Calculations with SOC

The coupling of the electron spin with orbital motion can induce strong SOC effects that may lead to an inverted band structure. In the systems Bi<sub>2</sub>Se<sub>3</sub>, Bi<sub>2</sub>Te<sub>3</sub>, and Sb<sub>2</sub>Te<sub>3</sub> this happens close to the Brillouin-zone center and is ultimately responsible for the topological properties of these materials, leading to the topologically protected surface and interface bands. The LDA results including spin-orbit interactions can be seen in Fig. 2 (red dashed lines). These band structures are in very good agreement with previous LDA calculations present in the literature (see, e.g., Refs. 20 and 22).

We have performed *GW* calculations using the full four-component spinor wave functions resulting from the SOC (green solid and blue dotted lines in Fig. 2). It can be clearly seen that in all cases the effective masses of the highest occupied and the lowest unoccupied bands are significantly affected by the quasiparticle corrections.

In contrast to the case of Sb<sub>2</sub>Te<sub>3</sub> without SOC, the *GW* correction does not lift the hybridization, which would reverse the order of bands and destroy the topological properties of the band structure. As we will show in more detail in Sec. III C, the inverted band structure remains intact also after the quasiparticle correction. However, the extent over which the band inversion takes place does change, in particular in the case of Bi<sub>2</sub>Te<sub>3</sub> where some *GW* (diag) bands—two valence

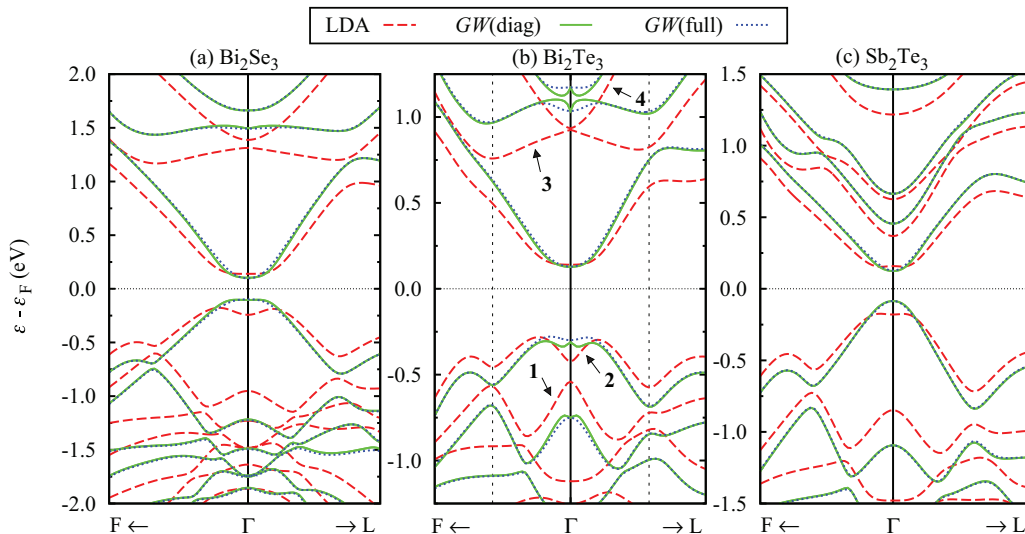


FIG. 2. (Color online) LDA,  $GW$  (diag), and  $GW$  (full) band structures of (a)  $\text{Bi}_2\text{Se}_3$ , (b)  $\text{Bi}_2\text{Te}_3$ , and (c)  $\text{Sb}_2\text{Te}_3$  with SOC. In panel (b), the labels 1, 2, 3, and 4 (pointing to the respective LDA bands) and the vertical dashed lines are a reference for Figs. 3 and 4.

bands labeled 1 and 2 and two conduction bands labeled 3 and 4—exhibit a peculiar, spiky dispersion close to the  $\Gamma$  point, again pointing at missing many-body hybridization effects. As in the previous section, this peculiar shape of the bands disappears when off-diagonal self-energy matrix elements are taken into account; the bands become smooth with a physically meaningful dispersion. The corresponding bands are shown as dotted-blue lines in Fig. 2. For the other systems and most of the other states of  $\text{Bi}_2\text{Te}_3$ , the off-diagonal elements of the self-energy do not lead to visible changes in the band structure, and the two approaches— $GW$  (diag) and  $GW$  (full)—yield almost identical results.

From Fig. 2(b) we can see that, in LDA, the states 1 and 2 as well as 3 and 4 of  $\text{Bi}_2\text{Te}_3$  are relatively close to each other at the  $\Gamma$  point. This gives rise to a pronounced hybridization between these two states. The  $GW$  quasiparticle correction separates the states energetically so that the hybridization changes. To account for this effect, the corresponding wave functions have to be given the freedom to change by inclusion of the off-diagonal self-energy matrix elements. The equivalent states in  $\text{Bi}_2\text{Se}_3$  and  $\text{Sb}_2\text{Te}_3$  are more separated in energy from the start, which explains why the unphysical spikes in the bands of Figs. 2(a) and 2(c) are so small that they are practically invisible on the scale of the figures.

It should be noted that the peculiar peaks in the spectrum of  $\text{Bi}_2\text{Te}_3$  were not observed in a previous  $GW$  calculation by Yazyev *et al.*,<sup>30</sup> because there the  $GW$  calculation was performed in the absence of SOC, in which these peculiar peaks are not present [see Fig. 1(b)], and the SOC was obtained at the LDA level and added to the QP spectrum *a posteriori*.

The inclusion of the off-diagonal elements of  $\Sigma$  also allows us to obtain the  $GW$  quasiparticle wave functions and, furthermore, study other properties that are derived from them (like the orbital character of the different states) and compare them to those from the LDA wave functions.

To gain more insight into the results of Fig. 2(b) and to analyze the hybridizations leading to the peculiar peaks observed in  $\text{Bi}_2\text{Te}_3$  within  $GW$  (diag), Fig. 3 shows the

$p$ -orbital projection of the wave functions corresponding to the bands of  $\text{Bi}_2\text{Te}_3$  labeled 1 and 2 in Fig. 2(b).

For the state labeled 2 (highest occupied band) the bismuth character increases when  $GW$  is applied and, in accordance, the tellurium character decreases. It is also visible that the region in  $\mathbf{k}$  space in which the Bi character is dominant is larger in  $GW$ . In other words, the band inversion is more extended in  $\mathbf{k}$  space, as we will also see in Sec. III C. Finally, to counterbalance the trend of band 2, the opposite effect is found for band 1.

A similar behavior is found for the bands labeled 3 and 4 in Fig. 2(b). Figure 4 represents the Te and Bi  $p$ -orbital character of these two bands. Band 4 has a dominant bismuth character in LDA [green dotted-dashed line in Fig. 4(b)], but around the  $\Gamma$  point the bismuth character decreases significantly and the tellurium character increases [Fig. 4(a)]. The opposite effect is found for band 3 (red solid lines). Thus there is a transfer of Bi character from band 4 to band 3, and of Te character

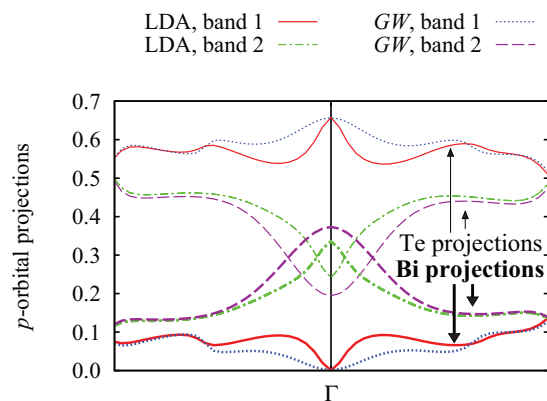


FIG. 3. (Color online) Tellurium (thin lines) and bismuth (thick lines)  $p$ -orbital character of the bands of  $\text{Bi}_2\text{Te}_3$  labeled 1 and 2 in Fig. 2(b) calculated using LDA and  $GW$  wave functions including SOC. The represented  $\mathbf{k}$  space corresponds to that between the vertical dashed lines in Fig. 2(b).

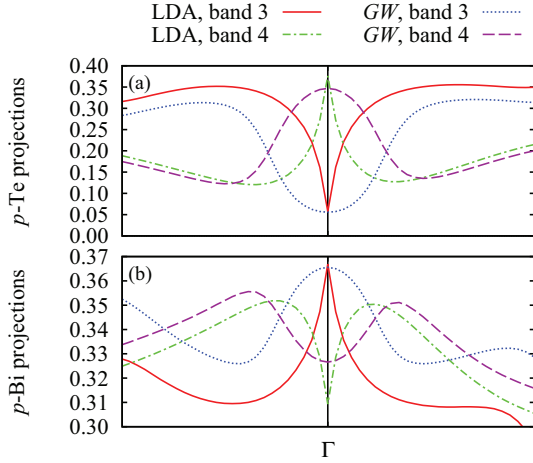


FIG. 4. (Color online) Same as Fig. 3 for the bands labeled 3 and 4 in Fig. 2(b). In this case, the (a) Te and (b) Bi projections are plotted separately.

from 3 to 4, giving rise to an avoided crossing. This avoided crossing is also visible in the  $GW$  projections, but in LDA it happens in a very small region of  $\mathbf{k}$  space, whereas for  $GW$  this region is more extended. This explains the much sharper LDA projections at  $\Gamma$  compared to the smoother  $GW$  ones. For other states of Bi<sub>2</sub>Te<sub>3</sub>, as well as for Bi<sub>2</sub>Se<sub>3</sub> and Sb<sub>2</sub>Te<sub>3</sub>, we find only small differences between the LDA and the  $GW$  projections.

### C. Analysis of the band inversion

Whereas the  $GW$  quasiparticle correction without SOC can roughly be described as a rigid shift of the conduction bands with respect to the valence bands (see Fig. 1), one observes clear changes in the band dispersions when SOC is included. We observe in Fig. 2 that the qualitative differences between LDA and  $GW$  are maximal for the highest valence band and the lowest conduction band. In particular, the “M shape” or “camelback shape” of the valence band, which is characteristic of the band inversion in these materials, flattens in the case of Bi<sub>2</sub>Te<sub>3</sub> and even disappears for Bi<sub>2</sub>Se<sub>3</sub> and Sb<sub>2</sub>Te<sub>3</sub>. This might give rise to doubts whether the  $GW$  approximation still predicts a band inversion for Bi<sub>2</sub>Se<sub>3</sub> and Sb<sub>2</sub>Te<sub>3</sub> as in DFT. In fact, a reversal of bands that had been found inverted in DFT was observed upon quasiparticle corrections for other families of materials in Ref. 48.

In order to analyze the band inversion in more detail, we have represented in Fig. 5 the projections of the LDA and  $GW$  wave functions onto the  $p$  states of Bi, Sb, Se, and Te. In all cases the  $GW$  calculations exhibit a band inversion in qualitative agreement with LDA, despite the flattening or disappearance of the M shape. For Bi<sub>2</sub>Te<sub>3</sub>, it is also visible that the region in  $\mathbf{k}$  space in which the band inversion occurs is larger in  $GW$ , in accordance with the projections shown in Fig. 3 for the band labeled 2.

Having calculated the quasiparticle wave functions explicitly also puts us in the position of making a statement about the effect of the  $GW$  quasiparticle correction on the  $Z_2$  topological invariants.<sup>1,4</sup> Only states of the same symmetry can have nonzero self-energy matrix elements. This implies

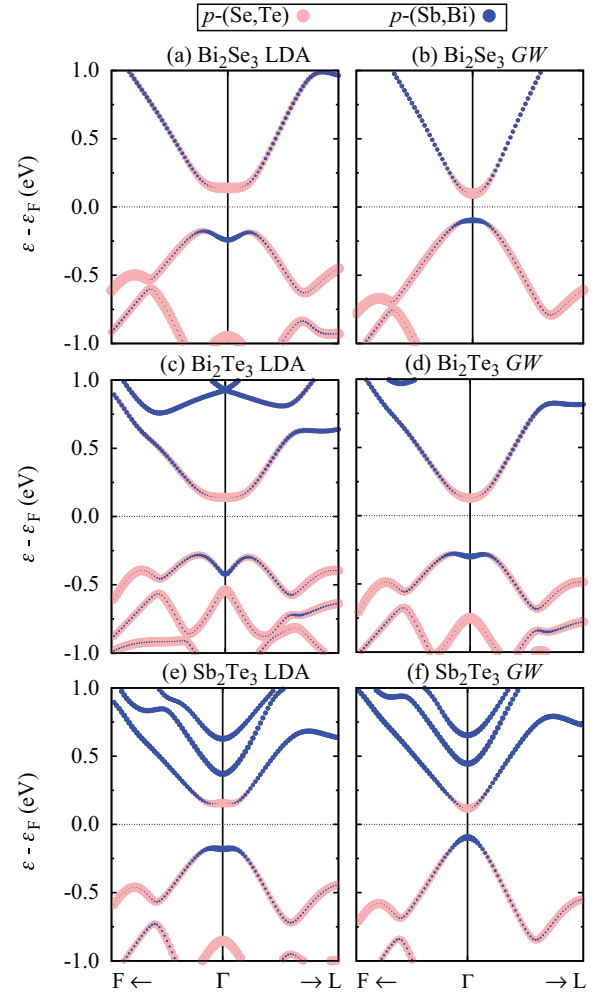


FIG. 5. (Color online) Projected band structures including SOC, calculated with LDA wave functions [(a), (c), and (e)] and  $GW$  quasiparticle wave functions [(b), (d), and (f)] for Bi<sub>2</sub>Se<sub>3</sub>, Bi<sub>2</sub>Te<sub>3</sub>, and Sb<sub>2</sub>Te<sub>3</sub>. The size of the circles is proportional to the projections of the wave functions onto the  $p$  states of the different species.

that  $\langle \phi_{\mathbf{k}\nu} | \Sigma(\omega) | \phi_{\mathbf{k}\nu'} \rangle = 0$  if the parity of the states  $\nu$  and  $\nu'$  differ. In other words, the parity of a wave function remains unchanged upon applying the  $GW$  quasiparticle correction. Thus the  $Z_2$  topological invariants could only change if we observed an interchange of valence and conduction states with respect to LDA at any of the time-reversal invariant momenta (TRIMs). This is not the case. Consequently, our  $GW$  calculations confirm the values of the  $Z_2$  topological invariants obtained previously with DFT.<sup>10</sup>

## IV. SUMMARY AND CONCLUSIONS

We have performed  $GW$  calculations for Bi<sub>2</sub>Se<sub>3</sub>, Bi<sub>2</sub>Te<sub>3</sub>, and Sb<sub>2</sub>Te<sub>3</sub> going beyond the widely used perturbative one-shot approach and analyzed the importance of off-diagonal elements of the self-energy matrix. For Sb<sub>2</sub>Te<sub>3</sub>, the LDA calculation without SOC shows a “negative” band gap (i.e., a wrong energy order of the two states determining the band gap). However, while correcting the sign of the band gap, i.e., making it positive, the perturbative

one-shot  $GW$  approach shows unphysical band dispersions, which—as we have shown—is a result of neglecting off-diagonal elements of the self-energy that couple different single-particle states, an effect that is not widely explored in the literature. Setting the off-diagonal matrix elements of the self-energy [or, more precisely, of  $\Sigma(\omega) - v_{xc}$ ] to zero disregards hybridization effects caused by many-body exchange and correlation. The hybridization is incomplete then. It misses a term that enables a mixing of the Kohn-Sham states, ultimately giving rise to the unphysical band dispersions.

We have shown that when SOC is fully taken into account, the off-diagonal elements of  $\Sigma$  introduce only small changes in the band structures of  $\text{Bi}_2\text{Se}_3$  and  $\text{Sb}_2\text{Te}_3$ , but they turn out to play a very important role in a small region around the  $\Gamma$  point in  $\text{Bi}_2\text{Te}_3$ , contrary to what is usually found for most bulk semiconductors.<sup>49,50</sup>

The importance of the off-diagonal self-energy matrix elements in  $\mathbf{k}$ -space regions of strong hybridization might have gone unnoticed in the past, as  $GW$  band structures are usually calculated and represented on a coarse  $\mathbf{k}$ -point mesh or using a Wannier interpolation,<sup>51</sup> where the avoided crossings are described by interpolation rather than by explicitly solving the quasiparticle equation on a dense  $\mathbf{k}$ -point grid. In the particular case of  $\text{Bi}_2\text{Te}_3$ , the effect found is only visible in a very small region around the  $\Gamma$  point, but not at the  $\Gamma$  point itself as can be understood from  $k \cdot p$  perturbation theory.<sup>10,30</sup> The importance

of the off-diagonal elements for  $\text{Bi}_2\text{Te}_3$  can, therefore, only be detected when a fine grid of  $\mathbf{k}$  points around  $\Gamma$  is used for calculating the band structures.

Whereas  $GW$  corrections without spin-orbit interactions can be described mainly as a rigid shift (except for the states discussed in Sec. III A determining the band gap of  $\text{Sb}_2\text{Te}_3$ ), we observed clear changes in the dispersions of the bands when SOC is included already in the reference system. These changes become larger close to the Fermi energy around the  $\Gamma$  point, in the region where the band inversion takes place. For  $\text{Bi}_2\text{Te}_3$ , the *camelback* shape of the valence band, which is characteristic of the band inversion, flattens significantly, and it disappears for  $\text{Bi}_2\text{Se}_3$  and  $\text{Sb}_2\text{Te}_3$ .

In order to determine whether, in spite of this, a band inversion is still present in  $GW$ , we have analyzed the band inversion in these materials based on the orbital character of the  $GW$  wave functions. According to our results, the band inversion persists, and the LDA values of the  $Z_2$  invariants remain unchanged upon applying quasiparticle corrections within the  $GW$  approximation.

## ACKNOWLEDGMENTS

This work was supported by the Alexander von Humboldt Foundation through a postdoctoral fellowship, and by the Helmholtz Association through the Virtual Institute for Topological Insulators (VITI).

- 
- <sup>1</sup>C. L. Kane and E. J. Mele, *Phys. Rev. Lett.* **95**, 146802 (2005).  
<sup>2</sup>B. A. Bernevig and S.-C. Zhang, *Phys. Rev. Lett.* **96**, 106802 (2006).  
<sup>3</sup>J. E. Moore and L. Balents, *Phys. Rev. B* **75**, 121306 (2007).  
<sup>4</sup>L. Fu and C. L. Kane, *Phys. Rev. B* **76**, 045302 (2007).  
<sup>5</sup>L. Fu, C. L. Kane, and E. J. Mele, *Phys. Rev. Lett.* **98**, 106803 (2007).  
<sup>6</sup>S. A. Wolf, D. D. Awschalom, R. A. Buhrman, J. M. Daughton, S. von Molnar, M. L. Roukes, A. Y. Chtchelkanova, and D. M. Treger, *Science* **294**, 1488 (2001).  
<sup>7</sup>L. Fu and C. L. Kane, *Phys. Rev. Lett.* **100**, 096407 (2008).  
<sup>8</sup>P. J. Leek, J. M. Fink, A. Blais, R. Bianchetti, M. Göppl, J. M. Gambetta, D. I. Schuster, L. Frunzio, R. J. Schoelkopf, and A. Wallraff, *Science* **318**, 1889 (2007).  
<sup>9</sup>P. Roushan, J. Seo, C. V. Parker, Y. S. Hor, D. Hsieh, D. Qian, A. Richardella, M. Z. Hasan, R. J. Cava, and A. Yazdani, *Nature (London)* **460**, 1106 (2009).  
<sup>10</sup>H. Zhang, C.-X. Liu, X.-L. Qi, X. Dai, Z. Fang, and S.-C. Zhang, *Nature Phys.* **5**, 438 (2009).  
<sup>11</sup>S. K. Mishra, S. Satpathy, and O. Jepsen, *J. Phys.: Condens. Matter* **9**, 461 (1997).  
<sup>12</sup>A. A. Bayaz, A. Giani, A. Foucaran, F. Pascal-Delannoy, and A. Boyer, *Thin Solid Films* **441**, 1 (2003).  
<sup>13</sup>C. L. Kane and E. J. Mele, *Phys. Rev. Lett.* **95**, 226801 (2005).  
<sup>14</sup>S. Murakami, *Phys. Rev. Lett.* **97**, 236805 (2006).  
<sup>15</sup>C.-X. Liu, X.-L. Qi, H.-J. Zhang, X. Dai, Z. Fang, and S.-C. Zhang, *Phys. Rev. B* **82**, 045122 (2010).  
<sup>16</sup>E. Mooser and W. B. Pearson, *Phys. Rev.* **101**, 492 (1956).  
<sup>17</sup>J. Black, E. M. Conwell, L. Seigle, and C. W. Spencer, *J. Phys. Chem. Solids* **2**, 240 (1957).  
<sup>18</sup>R. Sehr and L. R. Testardi, *J. Phys. Chem. Solids* **23**, 1219 (1962).  
<sup>19</sup>G. A. Thomas, D. H. Rapkine, R. B. V. Dover, L. F. Mattheiss, W. A. Sunder, L. F. Schneemeyer, and J. V. Waszczak, *Phys. Rev. B* **46**, 1553 (1992).  
<sup>20</sup>G. Wang and T. Cagin, *Phys. Rev. B* **76**, 075201 (2007).  
<sup>21</sup>B. Y. Yavorsky, N. F. Hinsche, I. Mertig, and P. Zahn, *Phys. Rev. B* **84**, 165208 (2011).  
<sup>22</sup>P. Larson, *Phys. Rev. B* **74**, 205113 (2006).  
<sup>23</sup>T. Thonhauser, T. J. Scheidemantel, J. O. Sofo, J. V. Badding, and G. D. Mahan, *Phys. Rev. B* **68**, 085201 (2003).  
<sup>24</sup>C. Pauly, G. Bihlmayer, M. Liebmann, M. Grob, A. Georgi, D. Subramaniam, M. R. Scholz, J. Sánchez-Barriga, A. Varykhalov, S. Blügel, O. Rader, and M. Morgenstern, *Phys. Rev. B* **86**, 235106 (2012).  
<sup>25</sup>L. Plucinski, A. Herdt, S. Fahrendorf, G. Bihlmayer, G. Mussler, S. Döring, J. Kampmeier, F. Matthes, D. E. Bürgler, D. Grützmacher, S. Blügel, and C. M. Schneider, *J. Appl. Phys.* **113**, 053706 (2013).  
<sup>26</sup>O. V. Yazyev, J. E. Moore, and S. G. Louie, *Phys. Rev. Lett.* **105**, 266806 (2010).  
<sup>27</sup>A. Herdt, L. Plucinski, G. Bihlmayer, G. Mussler, S. Döring, J. Krumrain, D. Grützmacher, S. Blügel, and C. M. Schneider, *Phys. Rev. B* **87**, 035127 (2013).  
<sup>28</sup>L. Hedin, *Phys. Rev.* **139**, A796 (1965).  
<sup>29</sup>E. Kioupakis, M. L. Tiago, and S. G. Louie, *Phys. Rev. B* **82**, 245203 (2010).

- <sup>30</sup>O. V. Yazyev, E. Kioupakis, J. E. Moore, and S. G. Louie, *Phys. Rev. B* **85**, 161101(R) (2012).
- <sup>31</sup>I. A. Nechaev, R. C. Hatch, M. Bianchi, D. Guan, C. Friedrich, I. Aguilera, J. L. Mi, B. B. Iversen, S. Blügel, P. Hofmann, and E. V. Chulkov, *Phys. Rev. B* **87**, 121111(R) (2013).
- <sup>32</sup>[www.flapw.de](http://www.flapw.de).
- <sup>33</sup>C. Friedrich, S. Blügel, and A. Schindlmayr, *Phys. Rev. B* **81**, 125102 (2010).
- <sup>34</sup>J. P. Perdew and A. Zunger, *Phys. Rev. B* **23**, 5048 (1981).
- <sup>35</sup>D. D. Koelling and B. N. Harmon, *J. Phys. C* **10**, 3107 (1977).
- <sup>36</sup>C. Li, A. J. Freeman, H. J. F. Jansen, and C. L. Fu, *Phys. Rev. B* **42**, 5433 (1990).
- <sup>37</sup>T. Kotani and M. van Schilfhaarde, *Solid State Commun.* **121**, 461 (2002).
- <sup>38</sup>C. Friedrich, A. Schindlmayr, S. Blügel, and T. Kotani, *Phys. Rev. B* **74**, 045104 (2006).
- <sup>39</sup>C. Friedrich, M. C. Müller, and S. Blügel, *Phys. Rev. B* **83**, 081101(R) (2011).
- <sup>40</sup>S. Nakajima, *J. Phys. Chem. Solids* **24**, 479 (1963).
- <sup>41</sup>R. W. G. Wyckoff, *Crystal Structures 2* (J. Wiley and Sons, New York, 1964).
- <sup>42</sup>T. L. Anderson and H. B. Krause, *Acta Crystallogr. B* **30**, 1307 (1974).
- <sup>43</sup>R. Sakuma, C. Friedrich, T. Miyake, S. Blügel, and F. Aryasetiawan, *Phys. Rev. B* **84**, 085144 (2011).
- <sup>44</sup>The spin-off-diagonal blocks of the self-energy should not be confused with the off-diagonal matrix elements of the self-energy that couple different electronic bands  $\nu \neq \nu'$ . The latter are the main subject of the present work. The former are caused by the fact that in the presence of SOC the spin is not a good quantum number anymore. So, even the diagonal self-energy matrix elements, i.e., taken with the same band index  $\nu = \nu'$ , have contributions from the spin-off-diagonal block of the self-energy.
- <sup>45</sup>R. W. Godby, M. Schlüter, and L. J. Sham, *Phys. Rev. B* **37**, 10159 (1988).
- <sup>46</sup>F. Aryasetiawan, in *Electronic Structure Calculations in Advances in Condensed Matter Science*, edited by V. I. Anisimov (Gordon and Breach, New York, 2000).
- <sup>47</sup>Since the quasiparticle energy  $\epsilon_{\mathbf{k}\nu}^{\text{QP}}$  appears on both sides of Eq. (1), as a (complex) eigenvalue on the right and as an argument to the self-energy on the left, we have to find a self-consistent solution in the sense that  $\epsilon_{\mathbf{k}\nu}^{\text{QP}}$  is an eigenvalue of the matrix  $\hat{T} + v_{\text{ext}} + v_{\text{H}} + \Sigma(\epsilon_{\mathbf{k}\nu}^{\text{QP}})$ . This procedure should not be confused with a self-consistent *GW* scheme (e.g., the quasiparticle self-consistent *GW* of Ref. 52) in which the self-energy is recalculated iteratively with updated *G* and *W* until convergence is reached.
- <sup>48</sup>J. Vidal, X. Zhang, L. Yu, J.-W. Luo, and A. Zunger, *Phys. Rev. B* **84**, 041109 (2011).
- <sup>49</sup>F. Aryasetiawan, *Phys. Rev. B* **46**, 13051 (1992).
- <sup>50</sup>A. Fleszar and W. Hanke, *Phys. Rev. B* **71**, 045207 (2005).
- <sup>51</sup>N. Marzari and D. Vanderbilt, *Phys. Rev. B* **56**, 12847 (1997).
- <sup>52</sup>S. V. Faleev, M. van Schilfhaarde, and T. Kotani, *Phys. Rev. Lett.* **93**, 126406, (2004).